Temperature-Dependent Structure of Epitaxial (Ba,Sr)TiO_3 Films Grown on $SrRuO_3$-Covered $SrTiO_3$ Substrates *

HE Jia-Qing(何佳清)[1,3**], E. VASCO[2], R. DITTMANN[3], WANG Ren-Hui(王仁卉)[1***]

[1]*Department of Physics and Center for Electron Microscopy, Wuhan University, Wuhan 430072*

[2]*Instituto de Ciencia de Materiales de Madrid, Consejo Superior de Investigaciones Científicas, 28049 Cantoblanco, Madrid, Spain*

[3]*Institut für Festkörperforschung, Forschungzentrum Jülich GmbH, D-52425 Jülich, Germany*

(Received 23 December 2005)

Growth dynamics of epitaxial (Ba,Sr)TiO_3 thin films deposited at different temperatures on $SrRuO_3/SrTiO_3$ substrates by pulsed laser deposition is investigated by transmission electron microscopy. The films exhibit a layered structure comprising sublayers with distinctive features in regard to the remaining strain, density of misfit dislocations and/or lattice defects, and growth habit. We correlate these temperature-dependent features with the predominant misfit-strain relaxation mechanisms for each one of the detected growth regimes. The thickness dependence of the film structure is discussed within the framework of the predictions for a kinetically modified Stranski–Krastanov growth mode.

PACS: 68. 37. lp, 68. 55. −a, 77. 55. +f

$Ba_{0.7}Sr_{0.3}TiO_3$ (BST hereafter) prepared in thin film form on $SrRuO_3$ (SRO)-covered $SrTiO_3$ (STO) is currently in the spotlight of the scientific community since outstanding dielectric properties (i.e., dielectric permittivities as high as $\varepsilon \approx 6600$)[1] have been verified for the epitaxial all-oxide SRO/BST/SRO/STO capacitor. These properties make BST attractive for an increasing number of applications, such as (i) new generations of store devices based on ultra high-density dynamic random access memory (DRAM) cells,[2] and (ii) high-performance microwave devices sustained on the tunability of BST dielectric properties via the Ba/Sr atomic ratio.[3] Beyond these exciting preliminary progresses, it is obvious that the dielectric properties of epitaxial BST are strongly affected[4] by the structure and stoichiometry (mainly the oxygen content) of the investigated films and therefore of limited reproducibility as these film features depend significantly on a large number of intrinsic and extrinsic parameters. The intrinsic parameters correspond to the thermodynamic characteristics (e.g., interface and free-surface energies, condensation energy, barriers for the formation of dislocations) of the system determining its growth dynamics, whereas the extrinsic ones are connected with kinetic limitations imposed by the processing conditions and the used deposition technique (e.g., the deposition rate, the substrate temperature, concentration of precursors). Far from equilibrium, the coexistence of both kinds of parameters through the competition between growth mechanisms determines the real growth mode of the films, and thus their atomic structure. Such a growth mode would roughly reproduce the system tendency toward minimum energy states (growth dynamics) that manifests via system transitions between close kinetic states, some of them metastable.[5] Thus, modified growth modes, unlike those predicted by classical theories for equilibrium surfaces (i.e., Frank–van-der-Merwe:[6] layer-by-layer growth; Volmer–Weber:[7] 3D-featured growth; and Stranski–Krastanov:[8] starting as 2D and then turning into 3D growth) would be feasible. These modified modes, where the dynamic and kinetic states coexist, are particularly attractive for novel applications:[9] e.g., as a nanostructuring tool.

In this Letter, we intend to shed light on how the growth kinetics modified through the substrate temperature of BST pulsed laser deposited on mismatched SRO/STO substrates influences on the growth dynamics (i.e., growth mode) of the epitaxial BST films. Our goal is to correlate the film structure with the deposition/processing conditions by means of identifying the underlying atomic mechanisms and the inherent features in the growth mode of epitaxial BST, with the ultimate purpose of establishing the basis for a future nanoengineering of perovskite oxides.

BST films were grown at different temperatures, namely 600, 700 and 800°C (±10°C), by pulsed-laser deposition (PLD), as described in Ref. [10]. Transmission electron microscopy (TEM) and high-resolution TEM (HRTEM) investigations were carried out in a Philips CM20-FEG and JEOL 4000EX microscopes.

Figures 1(a), 1(b), and 1(c) show the low-magnification cross-sectional TEM images of BST/SRO/STO heterostructures with 30–60-nm-thick BST films grown at 600, 700 and 800°C, respectively. The layered structure of the BST films extending from the atomically flat interface with the SRO bottom layer is clearly visible (as labelled). In particular, three sublayers are recognizable within the

* Supported by the National Natural Science Foundation of China and the Spanish Education and Science Ministry under the Ramón y Cajal Programme.

** Present address: Bldg. 480, Brookhaven National Laboratory, Upton NY-11973, USA; Email: jhe@bnl.gov

*** Email: rhwang@whu.edu.cn

©2006 Chinese Physical Society and IOP Publishing Ltd

film grown at 600°C (Fig. 1(a)): (i) A first 4-nm-thick sublayer (sublayer 1), which is mostly lattice defect-free layer as estimated from contrast absence, is directly seated on the BST/SRO interface. (ii) Beyond it, a second 10-nm-thick sublayer (2) exhibits a high density (high contrast) of defects and/or misfit dislocations. The compact structure of these two sublayers reveals their origin as the result of a 2D layer-by-layer growth regime. (iii) A third sublayer (3) extends from the inner interface with the second one throughout the rest of the BST film (about 45 nm). The latter shows a non-compact 3D columnar structure. The columns, which are single-crystalline, exhibit narrow size (i.e., width) and height distributions with an average size of 20 nm. They are separated from each other by broad (3 nm width) amorphous-like grain boundaries (denoted as A in Fig. 1(a)). Such boundaries extend along the growth direction, giving rise to approximately constant columnar cross sections and a smooth surface. A top-view image of the BST surface showing the morphology of the third sublayer (inset in Fig. 1(a)) reveals that the columns, seemingly by cross-sectional view, are uniform single-crystalline regions (dark regions), which are percolatively connected with each other and separated by interconnected boundary regions (lighted regions). The layered structure of the film grown at 700°C (Fig. 1(b)) is roughly similar to that of the film deposited at 600°C (i.e. it is comprised of three sublayers) except for the following features. (i) The crystalline quality of the sublayers and thus the entire film is higher as revealed by a lower density of dislocations and/or defects (lower contrast). (ii) The width of the boundary regions between single-crystalline columns shrinks down to a few lattices, and their appearance changes from amorphous-like to moderately disordered one such that they can be identified as planar defects.[10] (iii) The thickness of the defect-free interfacial layer (sublayer 1) decreases slightly down to 2.7–3 nm. Unlike those grown at 600 and 700°C, the BST films deposited at 800°C (Fig. 1(c)) exhibit only two sublayers, i.e., a defect-free 3-nm-thick interfacial sublayer followed by a 3D-featured columnar sublayer extending throughout the rest of the film. Both sublayers correspond roughly to the first and third one described above for the films grown at 600–700°C. In addition, major structural changes in the columnar sublayer are visible: (i) The columns, which are also single-crystalline, exhibit wide size and height distributions (with sizes ranging between 50 and 70 nm, and height variations giving place to a surface roughness of 7 nm for a 60-nm-thick film). (ii) The boundary regions, which look like those in the films grown at 700°C, glide down to the inner interface with the first sublayer, which explains why the second and third sublayer become a single one. The structure of this outermost sublayer is the outcome of a near-the-equilibrium 3D growth habit, which includes phenomena such as the migration and recrystallization of grain boundaries, the competition between coarsening grains, and the grain coalescence. Such a growth habit gives rise to the formation of equiaxial grains (as wide as height, which accounts for the size and height distributions found and) as those depicted in Fig. 1(c). In short, the films grown at 700°C exhibit the intermediate atomic structure of those detected in films deposited at 600°C and 800°C. Hence, these films show a layered structure (formed by three sublayers) similar to those obtained at lower temperatures (600°C) with crystalline qualities comparable to those achieved at higher temperatures (800°C).

Figures 2(a), 2(b), and 2(c) show the cross-sectional HRTEM images of the near BST/SRO interface regions for the BST films grown at 600, 700, and 800°C, respectively. These lattice images confirm the thickness dependence of the image contrast in Fig. 1. Independent of the growth temperature, the innermost sublayer (first sublayer) is free of misfit dislocations and/or lattice defects, forms a coherent interface with the SRO bottom layer, and then remains mostly strained. The interface of this sublayer with the above one is semi-coherent likely due to misfit strain relief taking place within the latter. Thus, beyond the thickness of the first sublayer (3–4 nm), misfit dislocations (pointed by vertical arrows in Figs. 2(a) and 2(c)), lattice planar defect (pointed by solid lines together with vertical arrow in Fig. 2(b)) and grain boundaries arise. By drawing a Burgers circuit (not shown here) enclosing the core of a misfit dislocation at the inner interface between the first and second sublayer in Fig. 2(a), the dislocation is identified as a perfect edge dislocation with a Burgers vector $a\langle 100\rangle$. The average spacing between dislocations measured along the inner interface (parallel to BST[010]) is larger than that estimated in Ref. [10] (about 25 nm) for a fully relaxed film where the lattice mismatch accommodates via the generation of $a\langle 010\rangle$ misfit dislocations. This result indicates that either the above sublayers remain partially strained or complementary strain relaxation mechanisms are operative. Such mechanisms would lead to a transition toward a 3D growth habit (according to the Stranski–Krastanov growth mode) via the formation of non-coherent grain boundaries, as that depicted in the inset of Fig. 2(a) for a film grown at 600°C. The contrast between the single-crystalline columns and the grain boundary regions is induced by lattice disorders and/or composition gradients. Hence, as previously reported in Ref. [11], the grain boundaries correspond to nonstoichiometric regions. An energy-dispersive x-ray spectroscopy (EDX) analysis (data not shown here) carried out on a large population of grain bulks, and grain boundaries reveals that the grain bulks exhibit atomic Ba/Sr ratios (Ba/Sr $\approx$ 2.2–2.4) close to that of the stoichiometric ceramic target ($Ba_{0.7}Sr_{0.3}TiO_3$) for PLD, whereas the grain boundary regions are Ba-depleted with the atomic ratio of Ba/Sr $\approx$ 1.

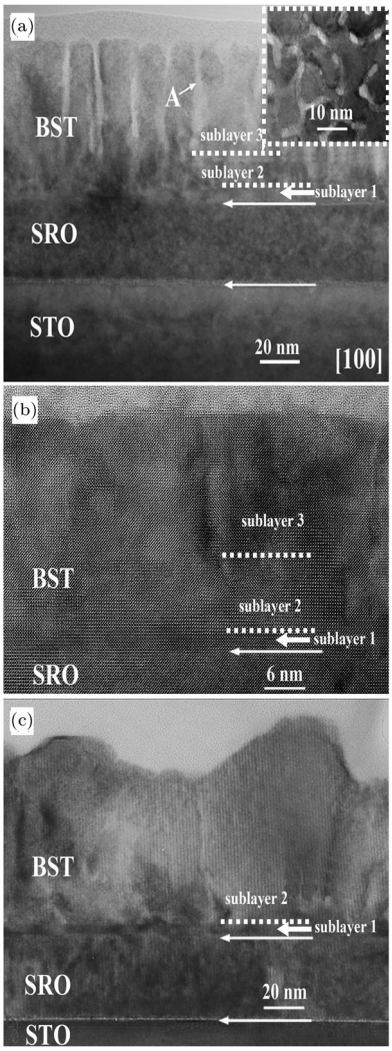


Fig. 1. Low-magnification cross-sectional images of BST/SRO/STO heterostructures with BST films grown at (a) 600°C, (b) 700°C, and (c) 800°C. The images are taken along [(a) and (b)] BST[100] and (c) BST[110] zone axes. The heterostructure interfaces are pointed by the horizontal arrows, whereas the BST sublayers are delimited by the dotted lines. Label A denotes grain boundary regions. Inset: plan-view image showing the morphology of the outermost sublayer for a film grown at 600°C.

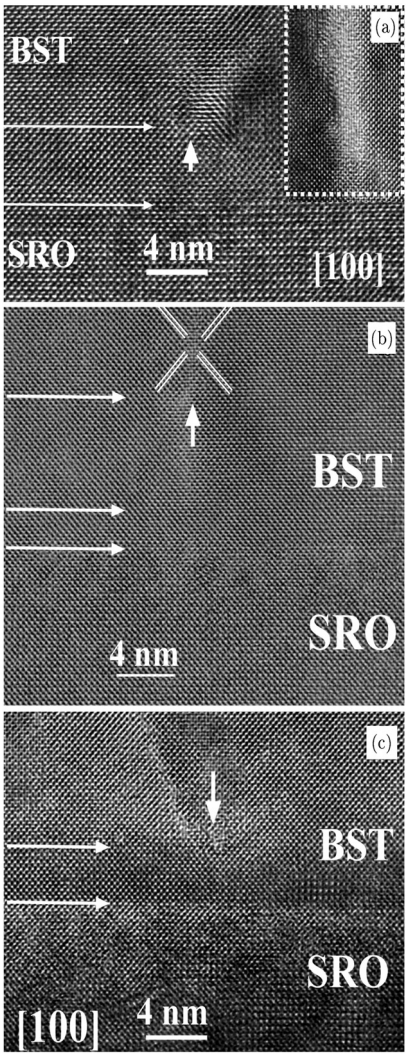


Fig. 2. High-magnification cross-sectional images BST/SRO interface regions for BST films growth at (a) 600°C, (b) 700°C, and (c) 800°C. All the images are taken along the BST[100] zone axes. The BST interfacial sublayer (the first sublayer) is delimited by the horizontal arrows, whereas misfit dislocations located at the inner interface are marked by the vertical ones. Inset in (a): cross sectional lattice image of the outermost sublayer for a BST film grown at 600°C.

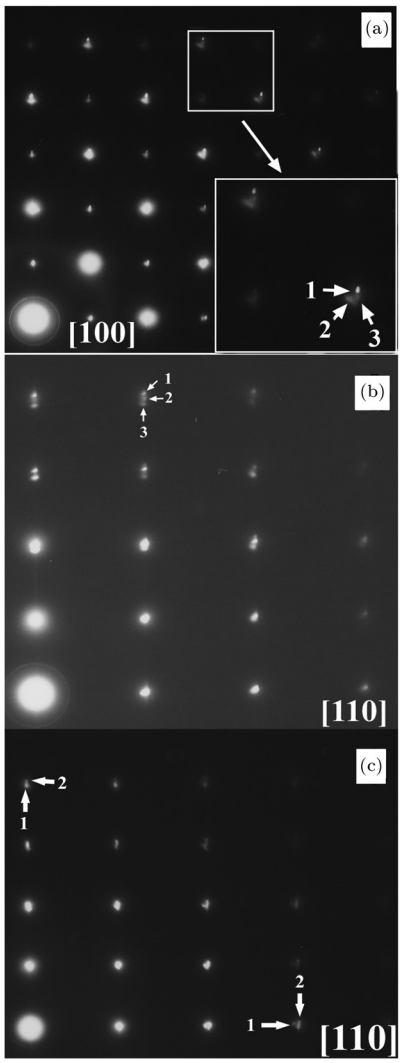


Fig. 3. SAED patterns recorded from cross-sectional specimens corresponding to the BST/SRO/STO heterostructures with the BST films grown at (a) 600°C, 700°C, and (b) 800°C. Inset in (a): the enlarged reciprocal space region around 044 diffractions with 1, 2 and 3 denoting the STO, BST and SRO 044 diffractions, respectively. The arrows labelled as 1, 2 and 3 in (b) correspond to the STO, SRO and BST $1\bar{1}4$ diffractions whereas those labelled as 1 and 2 in (c) identify diffraction spots of BST and SRO, respectively, in two orthogonal directions.

Figure 3 shows selected-area electron diffraction (SAED) patterns taken by means of an aperture that collects simultaneously diffractions coming from the BTO film, the SRO bottom layer and the STO substrate. Figures 3(a), 3(b), and 3(c) show the patterns recorded from cross-sectional specimens corresponding to the BST/SRO/STO heterostructures with the BST films grown at 600, 700, and 800°C, respectively. The region in the reciprocal space around 044 diffractions is magnified in the inset of Fig. 3(a). Three split diffraction spots, denoted by 1, 2, and 3 as sorted by decreasing intensities, are clearly distinguishable in the pattern plotted in Fig. 3(a), whose zone axis is parallel to BST[100]. The highest intensity spot (labelled as 1) is indexed as STO 044 diffraction by assuming STO lattice parameter $a_{\mathrm{STO}} = 0.3905$ nm. The middle intensity spot (2) is identified as 044 diffraction corresponding to the BST tetragonal lattice, whose in-plane and out-of-the-plane parameters are estimated to be $a_{\mathrm{BST}} = 0.3972$ nm and $c_{\mathrm{BST}} = 0.3980$ nm (unit cell tetragonality $c_{\mathrm{BST}}/a_{\mathrm{BST}} \approx 1.002$), respectively. The lowest intensity spot (3) is ascribed to the pseudo-

cubic SRO ($a_{SRO} = 0.3924$ nm) 044 diffraction. The elongation of spot 2 indicates a slight in-plane misalignment of a reduced fraction of BST columns. Three split diffraction spots along in-plane direction (parallel to BST[1$\bar{1}$0]) and two along the out-of-the-plane direction (parallel to BST[001]) were detected in the pattern depicted in Fig. 3(b) (zone axis parallel to BST[110]). The formers were sorted by decreasing intensities as 1, 2 and 3 and identified as 1$\bar{1}$4 diffractions corresponding to cubic STO, pseudo-cubic SRO and tetragonal BST, respectively. The BST lattice parameters ($a_{BST} = 0.3935$ nm and $c_{BST} = 0.4032$ nm) calculated from the SAED pattern and compared with those obtained for the film grown at 600°C (see above) reveal a higher remaining strain level in the film deposited at 700°C. Figure 3(c) shows an SAED pattern (zone axis parallel to BST[110]) taken with a narrower aperture such that only SRO and BST diffractions are collected, in which two split diffraction spots are detected along both the in-plane and out-of-the-plane directions. These spots denoted 1 and 2 are ascribed to BST and SRO, respectively. The computed BST lattice parameters ($a_{BST} = 0.3976$ nm and $c_{BST} = 0.3978$ nm) suggest a mostly relaxed film with lattice parameters close to those expected for the bulk-like perovskite $Ba_{0.7}Sr_{0.3}TiO_3$ (with $c_{BST} = 0.3977$ nm for a fully relaxed 200-nm-thick BST film[1]). Thus, the temperature evolution of BST lattice parameters indicates a net decrease (non-monotonous) of the remaining strain level in the films as the growth temperature rises. A state of high strain is found at intermediate temperatures where the kinetic limitations and the system dynamics are balanced, giving rise to an intermediate atomic structure as that observed in the films grown at 700°C.

According to the results shown above, BST epitaxially grown on SRO/STO by PLD follows a modified Stranski–Krastanov growth mode with certain temperature-dependent peculiarities. These peculiarities are originated by the prevailing strain relaxation mechanisms, which appear progressively during the growth as a function of the system energy balance and the operating kinetic limitations. Thus, the three sublayers detected within the BST films grown at 600–700°C correspond to different growth regimes (details in Ref. [11]), each one ruled by a distinctive strain relaxation mechanism (the first sublayer: point defects and/or surface perturbations; second: misfit dislocations; and the third one: grain boundaries) with typical activation energy (increasing as the sublayer index increases) and a characteristic level of remaining strain (the first sublayer: mostly strained; second: moderate strained; and the third one: mostly relaxed). The fusion of the second and third sublayer in a single sublayer (the outermost one) for films grown at higher temperatures (here 800°C) can be addressed as follows. Since the resulting sublayer retains the structural features of the third one (i.e. it exhibits a 3D-featured growth habit), the disappearance of the second sublayer as the growth temperature rises underlines its kinetic nature. Hence, the second sublayer is the outcome of a kinetically limited growth regime, which occurs at lower temperatures (600–700°C) than the temperature threshold for enabling the formation and migration of grain boundaries in films thinner than 14 nm. Two factors contribute to the disappearance of the second sublayer by increasing the strain level (at constant thickness), which must be released: (i) The BST/SRO lattice mismatch increases as the growth temperature increases (from about -1.7% at 600°C to about 1.9% at 800°C) due to the difference between the thermal expansion coefficients of both oxides (namely BST[3] $\alpha \approx 10.5 \times 10^{-6}\,K^{-1}$ and SRO[12] $\alpha \approx 5.2 \times 10^{-6}\,K^{-1}$); (ii) the decrease of the density of grain boundaries pertains to the grain coarsening via recrystallization and/or coalescence. The limited effectiveness of the misfit dislocations to release the thermally induced further strain produces a decrease of the crossover thickness (and consequently, a partial or total shrinkage of the second sublayer) for the transition toward the 3D-featured growth habit.

In conclusion, the influence of the kinetics on the growth dynamics of epitaxial BST films deposited on mismatched SRO/STO substrates by PLD has been investigated by TEM. The results allow us to correlate in a reliable way deposition and processing parameters (such as growth temperature) with the distinctive features of the layered structure of the films once the predominant misfit-strain relaxation mechanism identified. Such a mechanism induces the resulting growth mode (i.e. a distinctive atomic structure with a characteristic remaining strain level and typical densities of dislocations, grain boundaries and/or other lattice defects) for film thicknesses comprised of well-defined ranges, which are determined by the system energy balance and the operating kinetic limitations.

References

[1] Dittmann R et al 2003 *Appl. Phys. Lett.* **83** 5011
[2] Gao H J et al 1999 *Appl. Phys. Lett.* **75** 2542
Kuo S Y and Hsieh W F 2001 *Phys. Rev.* B **64** 224103
Abe K 2001 *J. Ceramic Soc. Jpn.* **109** S58
[3] Kim W J et al 2000 *Appl. Phys.* A **70** 313
[4] He J Q, Vasco E, Jia C L and Wang R H 2005 *Appl. Phys. Lett.* **87** 062901
[5] Snyder C W, Orr B G, Kessler D and Sander L M 1991 *Phys. Rev. Lett.* **66** 3032
[6] Frank F C and van der Merwe J H 1949 *Proc. Roy. Soc. London* A **198** 205
[7] Volmer M and Weber A 1926 *Z. Phys. Chem.* **119** 277
[8] Stranski I N and von Krastanov L 1939 *Akad. Wiss. Lit. Mainz Abh. Math. Naturwiss. Kl. IIb* **146** 797
[9] Mo Y W, Savage D E, Swartzentruber B S and Lagally M G 1990 *Phys. Rev. Lett.* **65** 1020
[10] He J Q et al 2005 *J. Appl. Phys.* **97** 104907
[11] He J Q, Vasco E, Dittmann R and Wang R H 2006 *Phys. Rev.* B **73** 125413
[12] López L L et al 2000 *Thin Solid Films* **373** 49